Measurement of the Born cross sections for $e^+e^- \to D_s^+ D_{s1}(2460)^- + \mathrm{c.c.}$ and $e^+e^- \to D_s^{*+} D_{s1}(2460)^- + \mathrm{c.c.}$

M. Ablikim,[1] M. N. Achasov,[10,d] P. Adlarson,[64] S. Ahmed,[15] M. Albrecht,[4] A. Amoroso,[63a,63c] Q. An,[60,48] Anita,[21] Y. Bai,[47] O. Bakina,[29] R. Baldini Ferroli,[23a] I. Balossino,[24a] Y. Ban,[38,l] K. Begzsuren,[26] J. V. Bennett,[5] N. Berger,[28] M. Bertani,[23a] D. Bettoni,[24a] F. Bianchi,[63a,63c] J. Biernat,[64] J. Bloms,[57] A. Bortone,[63a,63c] I. Boyko,[29] R. A. Briere,[5] H. Cai,[65] X. Cai,[1,48] A. Calcaterra,[23a] G. F. Cao,[1,52] N. Cao,[1,52] S. A. Cetin,[51b] J. F. Chang,[1,48] W. L. Chang,[1,52] G. Chelkov,[29,b,c] D. Y. Chen,[6] G. Chen,[1] H. S. Chen,[1,52] M. L. Chen,[1,48] S. J. Chen,[36] X. R. Chen,[25] Y. B. Chen,[1,48] W. Cheng,[63c] G. Cibinetto,[24a] F. Cossio,[63c] X. F. Cui,[37] H. L. Dai,[1,48] J. P. Dai,[42,h] X. C. Dai,[1,52] A. Dbeyssi,[15] R. B. de Boer,[4] D. Dedovich,[29] Z. Y. Deng,[1] A. Denig,[28] I. Denysenko,[29] M. Destefanis,[63a,63c] F. De Mori,[63a,63c] Y. Ding,[34] C. Dong,[37] J. Dong,[1,48] L. Y. Dong,[1,52] M. Y. Dong,[1,48,52] S. X. Du,[68] J. Fang,[1,48] S. S. Fang,[1,52] Y. Fang,[1] R. Farinelli,[24a,24b] L. Fava,[63b,63c] F. Feldbauer,[4] G. Felici,[23a] C. Q. Feng,[60,48] M. Fritsch,[4] C. D. Fu,[1] Y. Fu,[1] X. L. Gao,[60,48] Y. Gao,[61] Y. Gao,[38,l] Y. G. Gao,[6] I. Garzia,[24a,24b] E. M. Gersabeck,[55] A. Gilman,[56] K. Goetzen,[11] L. Gong,[37] W. X. Gong,[1,48] W. Gradl,[28] M. Greco,[63a,63c] L. M. Gu,[36] M. H. Gu,[1,48] S. Gu,[2] Y. T. Gu,[13] C. Y. Guan,[1,52] A. Q. Guo,[22] L. B. Guo,[35] R. P. Guo,[40] Y. P. Guo,[28] Y. P. Guo,[9,i] A. Guskov,[29] S. Han,[65] T. T. Han,[41] T. Z. Han,[9,i] X. Q. Hao,[16] F. A. Harris,[53] K. L. He,[1,52] F. H. Heinsius,[4] T. Held,[4] Y. K. Heng,[1,48,52] M. Himmelreich,[11,g] T. Holtmann,[4] Y. R. Hou,[52] Z. L. Hou,[1] H. M. Hu,[1,52] J. F. Hu,[42,h] T. Hu,[1,48,52] Y. Hu,[1] G. S. Huang,[60,48] L. Q. Huang,[61] X. T. Huang,[41] Z. Huang,[38,l] N. Huesken,[57] T. Hussain,[62] W. Ikegami Andersson,[64] W. Imoehl,[22] M. Irshad,[60,48] S. Jaeger,[4] S. Janchiv,[26,k] Q. Ji,[1] Q. P. Ji,[16] X. B. Ji,[1,52] X. L. Ji,[1,48] H. B. Jiang,[41] X. S. Jiang,[1,48,52] X. Y. Jiang,[37] J. B. Jiao,[41] Z. Jiao,[18] S. Jin,[36] Y. Jin,[54] T. Johansson,[64] N. Kalantar-Nayestanaki,[31] X. S. Kang,[34] R. Kappert,[31] M. Kavatsyuk,[31] B. C. Ke,[43,1] I. K. Keshk,[4] A. Khoukaz,[57] P. Kiese,[28] R. Kiuchi,[1] R. Kliemt,[11] L. Koch,[30] O. B. Kolcu,[51b,f] B. Kopf,[4] M. Kuemmel,[4] M. Kuessner,[4] A. Kupsc,[64] M. G. Kurth,[1,52] W. Kühn,[30] J. J. Lane,[55] J. S. Lange,[30] P. Larin,[15] L. Lavezzi,[63c] H. Leithoff,[28] M. Lellmann,[28] T. Lenz,[28] C. Li,[39] C. H. Li,[33] Cheng Li,[60,48] D. M. Li,[68] F. Li,[1,48] G. Li,[1] H. B. Li,[1,52] H. J. Li,[9,i] J. L. Li,[41] J. Q. Li,[4] Ke Li,[1] L. K. Li,[1] Lei Li,[3] P. L. Li,[60,48] P. R. Li,[32] S. Y. Li,[50] W. D. Li,[1,52] W. G. Li,[1] X. H. Li,[60,48] X. L. Li,[41] Z. B. Li,[49] Z. Y. Li,[49] H. Liang,[1,52] H. Liang,[60,48] Y. F. Liang,[45] Y. T. Liang,[25] L. Z. Liao,[1,52] J. Libby,[21] C. X. Lin,[49] B. Liu,[42,h] B. J. Liu,[1] C. X. Liu,[1] D. Liu,[60,48] D. Y. Liu,[42,h] F. H. Liu,[44] Fang Liu,[1] Feng Liu,[6] H. B. Liu,[13] H. M. Liu,[1,52] Huanhuan Liu,[1] Huihui Liu,[17] J. B. Liu,[60,48] J. Y. Liu,[1,52] K. Liu,[1] K. Y. Liu,[34] Ke Liu,[6] L. Liu,[60,48] Q. Liu,[52] S. B. Liu,[60,48] Shuai Liu,[46] T. Liu,[1,52] X. Liu,[32] Y. B. Liu,[37] Z. A. Liu,[1,48,52] Z. Q. Liu,[41] Y. F. Long,[38,l] X. C. Lou,[1,48,52] F. X. Lu,[16] H. J. Lu,[18] J. D. Lu,[1,52] J. G. Lu,[1,48] X. L. Lu,[1] Y. Lu,[1] Y. P. Lu,[1,48] C. L. Luo,[35] M. X. Luo,[67] P. W. Luo,[49] T. Luo,[9,i] X. L. Luo,[1,48] S. Lusso,[63c] X. R. Lyu,[52] F. C. Ma,[34] H. L. Ma,[1] L. L. Ma,[41] M. M. Ma,[1,52] Q. M. Ma,[1] R. Q. Ma,[1,52] R. T. Ma,[52] X. N. Ma,[37] X. X. Ma,[1,52] X. Y. Ma,[1,48] Y. M. Ma,[41] F. E. Maas,[15] M. Maggiora,[63a,63c] S. Maldaner,[28] S. Malde,[58] Q. A. Malik,[62] A. Mangoni,[23b] Y. J. Mao,[38,l] Z. P. Mao,[1] S. Marcello,[63a,63c] Z. X. Meng,[54] J. G. Messchendorp,[31] G. Mezzadri,[24a] T. J. Min,[36] R. E. Mitchell,[22] X. H. Mo,[1,48,52] Y. J. Mo,[6] N. Yu. Muchnoi,[10,d] H. Muramatsu,[56] S. Nakhoul,[11,g] Y. Nefedov,[29] F. Nerling,[11,g] I. B. Nikolaev,[10,d] Z. Ning,[1,48] S. Nisar,[8,j] S. L. Olsen,[52] Q. Ouyang,[1,48,52] S. Pacetti,[23b] X. Pan,[46] Y. Pan,[55] A. Pathak,[1] P. Patteri,[23a] M. Pelizaeus,[4] H. P. Peng,[60,48] K. Peters,[11,g] J. Pettersson,[64] J. L. Ping,[35] R. G. Ping,[1,52] A. Pitka,[4] R. Poling,[56] V. Prasad,[60,48] H. Qi,[60,48] H. R. Qi,[50] M. Qi,[36] T. Y. Qi,[9,*] S. Qian,[1,48] W.-B. Qian,[52] Z. Qian,[49] C. F. Qiao,[52] L. Q. Qin,[12] X. P. Qin,[13] X. S. Qin,[4] Z. H. Qin,[1,48] J. F. Qiu,[1] S. Q. Qu,[37] K. H. Rashid,[62] K. Ravindran,[21] C. F. Redmer,[28] A. Rivetti,[63c] V. Rodin,[31] M. Rolo,[63c] G. Rong,[1,52] Ch. Rosner,[15] M. Rump,[57] A. Sarantsev,[29,e] M. Savrié,[24b] Y. Schelhaas,[28] C. Schnier,[4] K. Schoenning,[64] D. C. Shan,[46] W. Shan,[19] X. Y. Shan,[60,48] M. Shao,[60,48] C. P. Shen,[9] P. X. Shen,[37] X. Y. Shen,[1,52] H. C. Shi,[60,48] R. S. Shi,[1,52] X. Shi,[1,48] X. D. Shi,[60,48] J. J. Song,[41] Q. Q. Song,[60,48] W. M. Song,[27] Y. X. Song,[38,l] S. Sosio,[63a,63c] S. Spataro,[63a,63c] F. F. Sui,[41] G. X. Sun,[1] J. F. Sun,[16] L. Sun,[65] S. S. Sun,[1,52] T. Sun,[1,52] W. Y. Sun,[35] Y. J. Sun,[60,48] Y. K. Sun,[60,48] Y. Z. Sun,[1] Z. T. Sun,[1] Y. H. Tan,[65] Y. X. Tan,[60,48] C. J. Tang,[45] G. Y. Tang,[1] J. Tang,[49] V. Thoren,[64] B. Tsednee,[26] I. Uman,[51d] B. Wang,[1] B. L. Wang,[52] C. W. Wang,[36] D. Y. Wang,[38,l] H. P. Wang,[1,52] K. Wang,[1,48] L. L. Wang,[1] M. Wang,[41] M. Z. Wang,[38,l] Meng Wang,[1,52] W. H. Wang,[65] W. P. Wang,[60,48] X. Wang,[38,l] X. F. Wang,[32] X. L. Wang,[9,i] Y. Wang,[49] Y. Wang,[60,48] Y. D. Wang,[15] Y. F. Wang,[1,48,52] Y. Q. Wang,[1] Z. Wang,[1,48] Z. Y. Wang,[1] Ziyi Wang,[52] Zongyuan Wang,[1,52] D. H. Wei,[12] P. Weidenkaff,[28] F. Weidner,[57] S. P. Wen,[1] D. J. White,[55] U. Wiedner,[4] G. Wilkinson,[58] M. Wolke,[64] L. Wollenberg,[4] J. F. Wu,[1,52] L. H. Wu,[1] L. J. Wu,[1,52] X. Wu,[9,i] Z. Wu,[1,48] L. Xia,[60,48] H. Xiao,[9,i] S. Y. Xiao,[1] Y. J. Xiao,[1,52] Z. J. Xiao,[35] X. H. Xie,[38,l] Y. G. Xie,[1,48] Y. H. Xie,[6] T. Y. Xing,[1,52] X. A. Xiong,[1,52] G. F. Xu,[1] J. J. Xu,[36] Q. J. Xu,[14] W. Xu,[1,52] X. P. Xu,[46] L. Yan,[9,i] L. Yan,[63a,63c] W. B. Yan,[60,48] W. C. Yan,[68] Xu Yan,[46] H. J. Yang,[42,h] H. X. Yang,[1] L. Yang,[65] R. X. Yang,[60,48] S. L. Yang,[1,52] Y. H. Yang,[36] Y. X. Yang,[12] Yifan Yang,[1,52] Zhi Yang,[25] M. Ye,[1,48] M. H. Ye,[7] J. H. Yin,[1] Z. Y. You,[49] B. X. Yu,[1,48,52] C. X. Yu,[37] G. Yu,[1,52] J. S. Yu,[20,m] T. Yu,[61] C. Z. Yuan,[1,52] W. Yuan,[63a,63c] X. Q. Yuan,[38,l] Y. Yuan,[1] Z. Y. Yuan,[49] C. X. Yue,[33] A. Yuncu,[51b,a] A. A. Zafar,[62] Y. Zeng,[20,m] B. X. Zhang,[1] Guangyi Zhang,[16] H. H. Zhang,[49] H. Y. Zhang,[1,48] J. L. Zhang,[66] J. Q. Zhang,[4] J. W. Zhang,[1,48,52] J. Y. Zhang,[1] J. Z. Zhang,[1,52] Jianyu Zhang,[1,52] Jiawei Zhang,[1,52] L. Zhang,[1] Lei Zhang,[36] S. Zhang,[49] S. F. Zhang,[36] T. J. Zhang,[42,h] X. Y. Zhang,[41] Y. Zhang,[58] Y. H. Zhang,[1,48] Y. T. Zhang,[60,48] Yan Zhang,[60,48] Yao Zhang,[1] Yi Zhang,[9,i] Z. H. Zhang,[6] Z. Y. Zhang,[65] G. Zhao,[1] J. Zhao,[33] J. Y. Zhao,[1,52] J. Z. Zhao,[1,48] Lei Zhao,[60,48] Ling Zhao,[1] M. G. Zhao,[37] Q. Zhao,[1] S. J. Zhao,[68] Y. B. Zhao,[1,48] Y. X. Zhao Zhao,[25] Z. G. Zhao,[60,48] A. Zhemchugov,[29,b] B. Zheng,[61] J. P. Zheng,[1,48] Y. Zheng,[38,l] Y. H. Zheng,[52] B. Zhong,[35] C. Zhong,[61] L. P. Zhou,[1,52] Q. Zhou,[1,52] X. Zhou,[65] X. K. Zhou,[52] X. R. Zhou,[60,48] A. N. Zhu,[1,52] J. Zhu,[37] K. Zhu,[1] K. J. Zhu,[1,48,52] S. H. Zhu,[59] W. J. Zhu,[37] X. L. Zhu,[50] Y. C. Zhu,[60,48] Z. A. Zhu,[1,52] B. S. Zou,[1] and J. H. Zou[1]

(BESIII Collaboration)

[1]*Institute of High Energy Physics, Beijing 100049, People's Republic of China*
[2]*Beihang University, Beijing 100191, People's Republic of China*
[3]*Beijing Institute of Petrochemical Technology, Beijing 102617, People's Republic of China*
[4]*Bochum Ruhr-University, D-44780 Bochum, Germany*
[5]*Carnegie Mellon University, Pittsburgh, Pennsylvania 15213, USA*
[6]*Central China Normal University, Wuhan 430079, People's Republic of China*
[7]*China Center of Advanced Science and Technology, Beijing 100190, People's Republic of China*
[8]*COMSATS University Islamabad, Lahore Campus, Defence Road, Off Raiwind Road, 54000 Lahore, Pakistan*
[9]*Fudan University, Shanghai 200443, People's Republic of China*
[10]*G.I. Budker Institute of Nuclear Physics SB RAS (BINP), Novosibirsk 630090, Russia*
[11]*GSI Helmholtzcentre for Heavy Ion Research GmbH, D-64291 Darmstadt, Germany*
[12]*Guangxi Normal University, Guilin 541004, People's Republic of China*
[13]*Guangxi University, Nanning 530004, People's Republic of China*
[14]*Hangzhou Normal University, Hangzhou 310036, People's Republic of China*
[15]*Helmholtz Institute Mainz, Johann-Joachim-Becher-Weg 45, D-55099 Mainz, Germany*
[16]*Henan Normal University, Xinxiang 453007, People's Republic of China*
[17]*Henan University of Science and Technology, Luoyang 471003, People's Republic of China*
[18]*Huangshan College, Huangshan 245000, People's Republic of China*
[19]*Hunan Normal University, Changsha 410081, People's Republic of China*
[20]*Hunan University, Changsha 410082, People's Republic of China*
[21]*Indian Institute of Technology Madras, Chennai 600036, India*
[22]*Indiana University, Bloomington, Indiana 47405, USA*
[23a]*INFN Laboratori Nazionali di Frascati, I-00044, Frascati, Italy*
[23b]*INFN and University of Perugia, I-06100, Perugia, Italy*
[24a]*INFN Sezione di Ferrara, I-44122, Ferrara, Italy*
[24b]*University of Ferrara, I-44122, Ferrara, Italy*
[25]*Institute of Modern Physics, Lanzhou 730000, People's Republic of China*
[26]*Institute of Physics and Technology, Peace Ave. 54B, Ulaanbaatar 13330, Mongolia*
[27]*Jilin University, Changchun 130012, People's Republic of China*
[28]*Johannes Gutenberg University of Mainz, Johann-Joachim-Becher-Weg 45, D-55099 Mainz, Germany*
[29]*Joint Institute for Nuclear Research, 141980 Dubna, Moscow region, Russia*
[30]*Justus-Liebig-Universitaet Giessen, II. Physikalisches Institut, Heinrich-Buff-Ring 16, D-35392 Giessen, Germany*
[31]*KVI-CART, University of Groningen, NL-9747 AA Groningen, Netherlands*
[32]*Lanzhou University, Lanzhou 730000, People's Republic of China*
[33]*Liaoning Normal University, Dalian 116029, People's Republic of China*
[34]*Liaoning University, Shenyang 110036, People's Republic of China*
[35]*Nanjing Normal University, Nanjing 210023, People's Republic of China*
[36]*Nanjing University, Nanjing 210093, People's Republic of China*
[37]*Nankai University, Tianjin 300071, People's Republic of China*
[38]*Peking University, Beijing 100871, People's Republic of China*
[39]*Qufu Normal University, Qufu 273165, People's Republic of China*
[40]*Shandong Normal University, Jinan 250014, People's Republic of China*
[41]*Shandong University, Jinan 250100, People's Republic of China*
[42]*Shanghai Jiao Tong University, Shanghai 200240, People's Republic of China*
[43]*Shanxi Normal University, Linfen 041004, People's Republic of China*
[44]*Shanxi University, Taiyuan 030006, People's Republic of China*
[45]*Sichuan University, Chengdu 610064, People's Republic of China*
[46]*Soochow University, Suzhou 215006, People's Republic of China*

[47]*Southeast University, Nanjing 211100, People's Republic of China*
[48]*State Key Laboratory of Particle Detection and Electronics, Beijing 100049, Hefei 230026, People's Republic of China*
[49]*Sun Yat-Sen University, Guangzhou 510275, People's Republic of China*
[50]*Tsinghua University, Beijing 100084, People's Republic of China*
[51a]*Ankara University, 06100 Tandogan, Ankara, Turkey*
[51b]*Istanbul Bilgi University, 34060 Eyup, Istanbul, Turkey*
[51c]*Uludag University, 16059 Bursa, Turkey*
[51d]*Near East University, Nicosia, North Cyprus, Mersin 10, Turkey*
[52]*University of Chinese Academy of Sciences, Beijing 100049, People's Republic of China*
[53]*University of Hawaii, Honolulu, Hawaii 96822, USA*
[54]*University of Jinan, Jinan 250022, People's Republic of China*
[55]*University of Manchester, Oxford Road, Manchester, M13 9PL, United Kingdom*
[56]*University of Minnesota, Minneapolis, Minnesota 55455, USA*
[57]*University of Muenster, Wilhelm-Klemm-Str. 9, 48149 Muenster, Germany*
[58]*University of Oxford, Keble Rd, Oxford, UK OX13RH*
[59]*University of Science and Technology Liaoning, Anshan 114051, People's Republic of China*
[60]*University of Science and Technology of China, Hefei 230026, People's Republic of China*
[61]*University of South China, Hengyang 421001, People's Republic of China*
[62]*University of the Punjab, Lahore-54590, Pakistan*
[63a]*University of Turin, I-10125, Turin, Italy*
[63b]*University of Eastern Piedmont, I-15121, Alessandria, Italy*
[63c]*INFN, I-10125, Turin, Italy*
[64]*Uppsala University, Box 516, SE-75120 Uppsala, Sweden*
[65]*Wuhan University, Wuhan 430072, People's Republic of China*
[66]*Xinyang Normal University, Xinyang 464000, People's Republic of China*
[67]*Zhejiang University, Hangzhou 310027, People's Republic of China*
[68]*Zhengzhou University, Zhengzhou 450001, People's Republic of China*

(Received 12 May 2020; accepted 4 June 2020; published 24 June 2020)

The processes $e^+e^- \to D_s^+ D_{s1}(2460)^- + \mathrm{c.c.}$ and $e^+e^- \to D_s^{*+} D_{s1}(2460)^- + \mathrm{c.c.}$ are studied for the first time using data samples collected with the BESIII detector at the BEPCII collider. The Born cross sections of $e^+e^- \to D_s^+ D_{s1}(2460)^- + \mathrm{c.c.}$ at nine center-of-mass energies between 4.467 GeV and 4.600 GeV and those of $e^+e^- \to D_s^{*+} D_{s1}(2460)^- + \mathrm{c.c.}$ at $\sqrt{s} = 4.590$ GeV and 4.600 GeV are measured. No obvious charmonium or charmoniumlike structure is seen in the measured cross sections.

DOI: 10.1103/PhysRevD.101.112008

[*]Corresponding author.
shedarshian@buaa.edu.cn
[a]Also at Bogazici University, 34342 Istanbul, Turkey.
[b]Also at the Moscow Institute of Physics and Technology, Moscow 141700, Russia.
[c]Also at the Functional Electronics Laboratory, Tomsk State University, Tomsk, 634050, Russia.
[d]Also at the Novosibirsk State University, Novosibirsk, 630090, Russia.
[e]Also at the NRC "Kurchatov Institute", PNPI, 188300, Gatchina, Russia.
[f]Also at Istanbul Arel University, 34295 Istanbul, Turkey.
[g]Also at Goethe University Frankfurt, 60323 Frankfurt am Main, Germany.
[h]Also at Key Laboratory for Particle Physics, Astrophysics and Cosmology, Ministry of Education; Shanghai Key Laboratory for Particle Physics and Cosmology; Institute of Nuclear and Particle Physics, Shanghai 200240, People's Republic of China.
[i]Also at Key Laboratory of Nuclear Physics and Ion-beam Application (MOE) and Institute of Modern Physics, Fudan University, Shanghai 200443, People's Republic of China.
[j]Also at Harvard University, Department of Physics, Cambridge, Massachusetts 02138, USA.
[k]Present address: Institute of Physics and Technology, Peace Ave.54B, Ulaanbaatar 13330, Mongolia.
[l]Also at State Key Laboratory of Nuclear Physics and Technology, Peking University, Beijing 100871, People's Republic of China.
[m]School of Physics and Electronics, Hunan University, Changsha 410082, China.

I. INTRODUCTION

The charmed-strange mesons, known as D_s, are made up of $c\bar{s}$ or $\bar{c}s$ quarks. The $D_{s1}(2460)$ meson was first observed in 2003 by the CLEO experiment via its decay into $D_s^{*+}\pi^0$ [1]. It was subsequently confirmed by the Belle [2] and *BABAR* [3] experiments. The experimental results favor a $J^P = 1^+$ quantum number assignment for $D_{s1}(2460)$ as a P-wave state. However, its measured mass (2459.5 ± 0.6) MeV$/c^2$ is at least 70 MeV$/c^2$ lower than the quark model predictions [4,5], leading to an unexpectedly narrow width. It has also been proposed to be a good candidate for a D^*K molecule state [6–8], or a mixture of the $c\bar{s}$ and D^*K state [9].

The $D_{s1}(2460)$ can be produced in the processes $e^+e^- \to D_s^+ D_{s1}(2460)^- +$c.c. and $e^+e^- \to D_s^{*+} D_{s1}(2460)^- +$ c.c.. Following the excitation behavior of S-wave production, Ref. [10] predicts $\sigma[e^+e^- \to D_s^* D_{s0}^*(2317)]$ and $\sigma[e^+e^- \to D_s D_{s1}(2460)] \propto \sqrt{E_{\mathrm{c.m.}} - E_0}$, where $E_{\mathrm{c.m.}}$ is the center-of-mass (c.m.) energy and $E_0 \approx 4.43$ GeV is the mass threshold of both channels.

Additionally, several charmoniumlike Y states with $J^{PC} = 1^{--}$ lying above the open charm threshold have been discovered, such as the $Y(4260)$ [11–13], $Y(4360)$ [14,15], and $Y(4660)$ [15]. Measurements of these charmoniumlike states decaying into a charmed-antistrange and anticharmed-strange meson pair provide crucial insight on their internal structure. The Belle [16], *BABAR* [17], and CLEO [18] experiments have measured the cross sections of $e^+e^- \to D_s^{(*)}\bar{D}_s^{(*)}$ with low-lying charmed-strange mesons in the final states. Using an e^+e^- collision data sample corresponding to 567 pb^{-1} collected at $\sqrt{s} = 4.600$ GeV, the BESIII experiment has measured the cross section of $e^+e^- \to D_s^+\bar{D}^{(*)0}K^-$, which includes significant contributions from events with the $D_{s1}(2536)^-$ and $D_{s2}^*(2573)^-$ charmed-strange mesons [19]. Using a data sample of 921.9 fb^{-1} collected at $\sqrt{s} = 10.52$, 10.58, and 10.867 GeV, Belle measured the cross sections of $e^+e^- \to D_s^+ D_{s1}(2536)^-$ and $e^+e^- \to D_s^+ D_{s2}^*(2573)^-$ and observed the $Y(4626)$ with significances of 5.9σ and 3.4σ, respectively, with systematic uncertainties included [20,21].

In this paper, we report the first measurement of the Born cross sections for $e^+e^- \to D_s^+ D_{s1}(2460)^- +$ c.c. and $e^+e^- \to D_s^{*+} D_{s1}(2460)^- +$ c.c., and the search for possible vector charmoniumlike states. Throughout the paper, charged-conjugate modes are always implied.

II. DETECTOR, DATA SAMPLES AND MONTE CARLO SIMULATIONS

BESIII [22] and BEPCII are major upgrades of the BESII detector [23] and the BEPC accelerator. The cylindrical core of the BESIII detector consists of a helium-based multilayer drift chamber (MDC), a plastic scintillator time-of-flight system (TOF), and a CsI(Tl) electromagnetic calorimeter (EMC), which are all enclosed in a superconducting solenoidal magnet providing a 1.0 T magnetic field. The solenoid is supported by an octagonal flux-return yoke with resistive plate counter muon identifier modules interleaved with steel. The acceptance of charged particles and photons is 93% over 4π solid angle. The charged particle momentum resolution at 1 GeV/c is 0.5%, and the energy loss ($\mathrm{d}E/\mathrm{d}x$) resolution is 6% for the electrons from Bhabha scattering. The EMC photon energy resolution is 2.5% (5%) at 1 GeV in the barrel (end cap) region. The time resolution of the TOF barrel (end cap) is 68 ps (110 ps). Our particle identification (PID) methods combine the TOF information with the $\mathrm{d}E/\mathrm{d}x$ measured in the MDC to calculate the probability Prob(h), $h = \pi, K$, for a track to be a pion or a kaon.

In this paper, the Born cross sections of the processes $e^+e^- \to D_s^+ D_{s1}(2460)^-$ and $e^+e^- \to D_s^{*+} D_{s1}(2460)^-$ are measured for the first time at nine energy points between 4.467 and 4.600 GeV, and at 4.590 and 4.600 GeV, respectively. Table I lists the data samples used in this analysis and their integrated luminosities. The c.m. energies are measured using the process $e^+e^- \to \mu^+\mu^-$ with an uncertainty of 0.8 MeV [24]. The integrated luminosities are measured with an uncertainty of 1.0% using large-angle Bhabha scattering events [25,26].

The GEANT4-based [27] Monte Carlo (MC) simulation framework BOOST [28], which consists of event generators and the description of the detector geometry and response, is used to produce large simulated event samples. These are used to optimize the event selection criteria, determine the detection efficiency, evaluate the initial state radiation (ISR) correction factor $(1 + \delta)$, and estimate background contributions. The simulation includes the beam energy spread and ISR modeled with KKMC [29–31] and BesEvtGen [32,33]. The final state radiation (FSR) effects are simulated by the PHOTOS [34] package. For each energy point, we generate MC samples of the signal processes $e^+e^- \to D_s^+ D_{s1}(2460)^-$ and $e^+e^- \to D_s^{*+} D_{s1}(2460)^-$ with a uniform distribution in phase space (PHSP).

The signal process $e^+e^- \to D_s^+ D_{s1}(2460)^-$ is simulated with D_s^+ decaying into $K^+K^-\pi^+$, and the $D_{s1}(2460)^-$ decaying into all possible final states. The signal process $e^+e^- \to D_s^{*+} D_{s1}(2460)^-$ is simulated with D_s^{*+} decaying into γD_s^+ and the $D_{s1}(2460)^-$ decaying into all possible final states. A P-wave model and a Dalitz plot decay model [35] are used to simulate $D_s^{*+} \to \gamma D_s^+$ and $D_s^+ \to K^+K^-\pi^+$, respectively.

Two generic MC simulated samples at $\sqrt{s} = 4.575$ GeV and 4.600 GeV, equivalent to the respective integrated luminosity of each data set, are produced to investigate potential peaking background channels. Known processes and decay modes are generated by BesEvtGen with cross sections and branching fractions obtained from the Particle Data Group (PDG) [36]. The remaining unmeasured phenomena associated with charmonium decays or open

TABLE I. Summary of the measurements of the Born cross sections for $e^+e^- \to D_s^+ D_{s1}(2460)^-$ and $e^+e^- \to D_s^{*+} D_{s1}(2460)^-$. Listed in the table are the integrated luminosity $\mathcal{L}_{\rm int}$, the signal efficiency ϵ (ϵ^*) from signal MC samples, the number of fitted $D_{s1}(2460)^-$ signal events $N_{\rm fit}$, the 90% C.L. upper limit on the number of fitted $D_{s1}(2460)^-$ signal yields $N_{\rm U.L.}$, the ISR radiative correction factor $(1+\delta)$, the statistical signal significance, and the measured Born cross section σ_B and its 90% C.L. upper limit $\sigma_B^{\rm U.L.}$ (with systematic uncertainties included).

$\sqrt{s}$ (GeV)	$\mathcal{L}_{\rm int}$ (pb^{-1})	ϵ (ϵ^*)	$N_{\rm fit}$	$N_{\rm U.L.}$	$(1+\delta)$	Significance	σ_B ($\sigma_B^{\rm U.L.}$) (pb)
			$e^+e^- \to D_s^+ D_{s1}(2460)^- + {\rm c.c.}$				
4.467	111.1	32.8%	$3.0^{+9.8}_{-9.0}$	19.2	0.739	0.3σ	$1.9^{+6.3}_{-5.8}$ (15.3)
4.527	112.1	31.1%	40.0 ± 9.7	···	0.757	4.9σ	$26.3 \pm 6.4 \pm 2.7$
4.550	8.8	30.5%	$-0.7^{+4.2}_{-3.5}$	7.7	0.764	···	$-6.0^{+35.7}_{-29.8}$ (67.3)
4.560	8.3	30.2%	$-3.6^{+3.8}_{-2.9}$	6.1	0.769	···	$-32.6^{+34.4}_{-26.3}$ (62.4)
4.570	8.4	30.1%	$8.8^{+5.5}_{-4.7}$	17.1	0.780	2.0σ	$77.7^{+48.6}_{-41.5}$ (179)
4.575	48.9	32.2%	22.3 ± 7.6	···	0.788	3.5σ	$31.2 \pm 10.6 \pm 7.0$
4.580	8.6	29.9%	$-0.5^{+2.5}_{-4.7}$	6.6	0.798	···	$-4.3^{+21.3}_{-40.1}$ (63.9)
4.590	8.2	29.6%	$-3.4^{+3.6}_{-2.7}$	5.9	0.819	···	$-29.9^{+31.7}_{-23.8}$ (64.2)
4.600	586.9	31.8%	242.0 ± 22.9	···	0.847	13.7σ	$26.6 \pm 2.5 \pm 2.5$
			$e^+e^- \to D_s^{*+} D_{s1}(2460)^- + {\rm c.c.}$				
4.590	8.2	(13.0%)	$4.8^{+4.8}_{-2.7}$	9.9	0.818	2.0σ	$96.7^{+97.3}_{-54.7}$ (203)
4.600	586.9	(13.1%)	82.1 ± 15.9	···	0.847	5.9σ	$22.1 \pm 4.3 \pm 1.9$

charm processes are simulated with LUNDCHARM [32,37], while continuum light hadronic events are produced with PYTHIA [38].

III. COMMON SELECTION CRITERIA

The candidate events for $e^+e^- \to D_s^+ D_{s1}(2460)^-$ and $e^+e^- \to D_s^{*+} D_{s1}(2460)^-$ are selected with a partial reconstruction method to obtain higher efficiencies. The D_s^+ candidates are reconstructed via $D_s^+ \to \phi\pi^+$, $\phi \to K^+K^-$ and $D_s^+ \to \bar{K}^{*0}K^+$, $\bar{K}^{*0} \to K^-\pi^+$. The D_s^{*+} candidates are reconstructed via $D_s^{*+} \to \gamma D_s^+$. The $D_{s1}(2460)^-$ signals are identified with the mass recoiling against the reconstructed D_s^+ and D_s^{*+}. There are three charged tracks in $D_s^+ \to K^+K^-\pi^+$, and one additional photon candidate in $D_s^{*+} \to \gamma D_s^+$.

For each charged track candidate, the polar angle θ in the MDC with respect to the detector axis must satisfy $|\cos\theta| < 0.93$, and the point of closest approach to the e^+e^- interaction point must be within ± 10 cm in the beam direction and within 1 cm in the plane perpendicular to the beam direction. Pion candidates are required to satisfy ${\rm Prob}(\pi) > {\rm Prob}(K)$ and ${\rm Prob}(\pi) > 0.001$. Kaon candidates are required to satisfy ${\rm Prob}(K) > {\rm Prob}(\pi)$ and ${\rm Prob}(K) > 0.001$.

The photon candidates are selected from showers in the EMC. The deposited energy in the EMC is required to be larger than 25 MeV in the barrel region ($|\cos\theta| < 0.80$) or greater than 50 MeV in the endcap region ($0.86 < |\cos\theta| < 0.92$). To eliminate the showers produced by charged tracks, photon candidates must be separated by at least 20° from the extrapolated position of all charged tracks in the EMC. The timing of the shower is required to be within 700 ns from the reconstructed event start time to suppress noise and energy deposits unrelated to the event.

The candidate events of both $e^+e^- \to D_s^+ D_{s1}(2460)^-$ and $e^+e^- \to D_s^{*+} D_{s1}(2460)^-$ are required to contain at least two kaons and one pion. One additional photon candidate is required for $e^+e^- \to D_s^{*+} D_{s1}(2460)^-$. All combinations of $K^+K^-\pi^+$ that pass the vertex fit are kept. To select $D_s^+ \to \phi\pi^+, \phi \to K^+K^-$ and $D_s^+ \to \bar{K}^{*0}K^+$, $\bar{K}^{*0} \to K^-\pi^+$ submodes, the invariant masses of K^+K^- and $K^-\pi^+$ are required to satisfy $|M(K^+K^-) - m_\phi| < 15$ MeV$/c^2$ and $|M(K^-\pi^+) - m_{\bar{K}^{*0}}| < 84$ MeV$/c^2$, respectively, where m_ϕ ($m_{\bar{K}^{*0}}$) is the nominal mass of the ϕ ($\bar{K}^{*0}$) meson taken from the PDG [36].

IV. MEASUREMENT OF $e^+e^- \to D_s^+ D_{s1}(2460)^-$

To improve the resolution of the D_s^+ recoil mass, we define $M_{D_s^+}^{\rm rec} \equiv M_{K^+K^-\pi^+}^{\rm recoil} + M(K^+K^-\pi^+) - m_{D_s^+}$, where $M_{K^+K^-\pi^+}^{\rm recoil} = \sqrt{(P_{\rm c.m.} - P_{K^+} - P_{K^-} - P_{\pi^+})^2}$, $P_{\rm c.m.}$, P_{K^+}, P_{K^-}, and P_{π^+} are the four-momenta of the initial e^+e^- system, the selected K^+, K^-, and π^+, respectively, $M(K^+K^-\pi^+)$ is the invariant mass of the $K^+K^-\pi^+$ system, and $m_{D_s^+}$ is the nominal mass of the D_s^+ meson [36].

We separate the $M_{D_s^+}^{\rm rec}$ spectrum into 4.0 MeV$/c^2$ wide bins. We use 25 bins between 2.40 GeV$/c^2$ and 2.50 GeV$/c^2$ for the data samples taken at $\sqrt{s} = 4.467$ GeV, 4.527 GeV, and 4.575 GeV, and 35

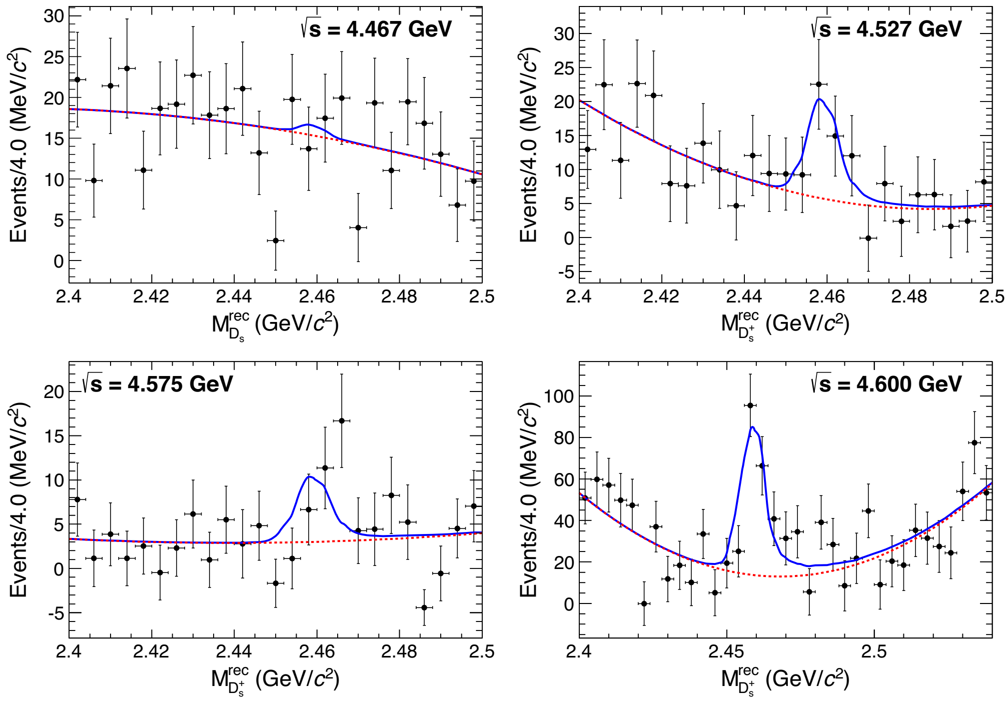

FIG. 1. $M^{\rm rec}_{D_s^+}$ distributions at $\sqrt{s} = 4.467$ GeV, 4.527 GeV, 4.575 GeV, and 4.600 GeV, respectively, obtained by extracting D_s^+ signal yields in the fit to the $M(K^+K^-\pi^+)$ distribution in each $M^{\rm rec}_{D_s^+}$ bin. The dots with error bars are data, the solid lines are the best fits, and the dashed lines are the fitted backgrounds. Clear $D_{s1}(2460)^-$ signals are seen at $\sqrt{s} = 4.527$ GeV, 4.575 GeV, and 4.600 GeV. The fitted results together with the signal significances are summarized in Table I.

bins between 2.40 GeV$/c^2$ and 2.54 GeV$/c^2$ for the data sample at $\sqrt{s} = 4.600$ GeV. An unbinned maximum likelihood fit is performed to the $M(K^+K^-\pi^+)$ distribution for events in each $M^{\rm rec}_{D_s^+}$ bin. The signal distribution is modeled by a Gaussian function, the parameters of which are fixed to those obtained from the fit to the original integrated $M(K^+K^-\pi^+)$ spectrum. The background shape is described by a first-order polynomial function. The obtained $M^{\rm rec}_{D_s^+}$ distributions, based on these fitted D_s^+ signal yields, are shown in Fig. 1 for four different energy points. Detailed studies of the generic MC samples [39] indicate that there are no peaking backgrounds in the $D_{s1}(2460)^-$ signal region. In the lower mass region the dominant backgrounds are from the process $e^+e^- \to D_s^{*+}D_s^{*-}$, while in the higher mass region the backgrounds are from processes with final states $D_s^+\bar{D}^{(*)0}K^-$, $D_s^+D^{(*)-}\bar{K}^0$, etc.

We fit these $M^{\rm rec}_{D_s^+}$ distributions to determine the signal yield of $D_{s1}(2460)^-$. The signal distribution is modeled by a MC-derived signal shape, while the background is described by a second-order polynomial. The fit results are shown in Fig. 1 and summarized in Table I. The significances of the $D_{s1}(2460)^-$ signals are determined from the changes in the log-likelihood values with and without inclusion of a $D_{s1}(2460)^-$ signal in the fit, taking the change of the number of degrees of freedom into account. We obtain significances larger than 3σ at $\sqrt{s} = 4.527$ GeV, 4.575 GeV, and 4.600 GeV. No significant $D_{s1}(2460)^-$ signal is observed in the data sample at $\sqrt{s} = 4.467$ GeV.

Due to the limited statistics, we employ a different strategy for the data samples at $\sqrt{s} = 4.550$ GeV, 4.560 GeV, 4.570 GeV, 4.580 GeV, and 4.590 GeV. In those cases, $M(K^+K^-\pi^+)$ is first required to satisfy $|M(K^+K^-\pi^+) - m_{D_s^+}| < 10$ MeV$/c^2$. A fit is then directly performed to the $M^{\rm rec}_{D_s^+}$ distributions, using a MC-derived $D_{s1}(2460)^-$ signal shape for the signal and a first-order polynomial for the background. The fit results are shown in Fig. 2. No significant $D_{s1}(2460)^-$ signals are observed in these five data samples. The fit results together with the signal significances are summarized in Table I.

Since the statistical significances of the $D_{s1}(2460)^-$ signal at some energy points are less than 3σ, the upper limits on the numbers of $D_{s1}(2460)^-$ signal events ($N_{\rm U.L.}$) are determined at the 90% confidence level (C.L.) by solving the following equation:

$$\int_0^{N_{\rm U.L.}} \mathcal{L}(x)dx = 0.9\int_0^{+\infty} \mathcal{L}(x)dx, \qquad (1)$$

where x is the assumed yield of $D_{s1}(2460)^-$ signal, and $\mathcal{L}(x)$ is the corresponding maximum likelihood from the data. The resulting $N_{\rm U.L.}$ obtained using the above method are listed in Table I.

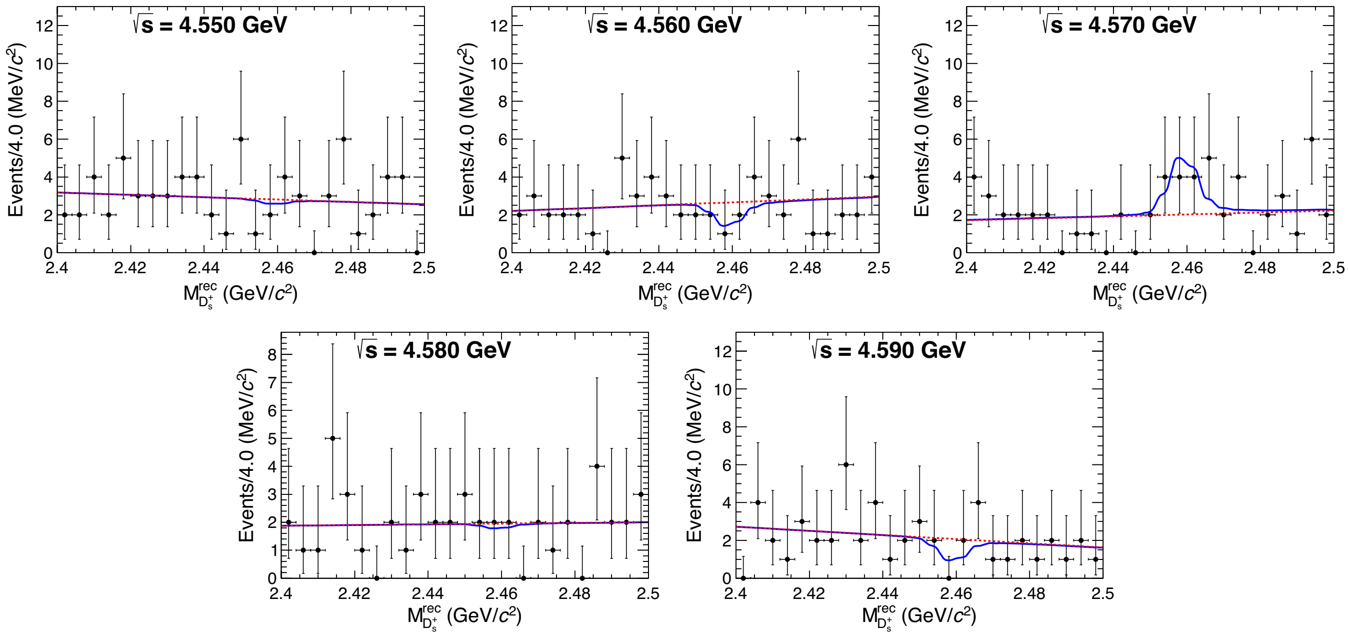

FIG. 2. $M^{\mathrm{rec}}_{D_s^+}$ distributions from data samples at $\sqrt{s} = 4.550$ GeV, 4.560 GeV, 4.570 GeV, 4.580 GeV, and 4.590 GeV. The dots with error bars are data, the solid lines are the best fits, and the dashed lines are the fitted backgrounds. The fitted results together with the signal significances are summarized in Table I.

The Born cross section of $e^+e^- \to D_s^+ D_{s1}(2460)^-$ is calculated using the formula:

$$\sigma_B(e^+e^- \to D_s^+ D_{s1}(2460)^-) = \frac{N_{\mathrm{fit}}}{\mathcal{L}_{\mathrm{int}}(1+\delta)(1+\delta^{\mathrm{vp}})\epsilon_{D_s}}, \tag{2}$$

where N_{fit} is the $D_{s1}(2460)^-$ signal yield, $1+\delta$ is the radiative correction factor obtained from a QED calculation with 1% accuracy [40] using the KKMC generator, $1+\delta^{\mathrm{vp}}$ is the vacuum polarization factor, whose calculations are from Ref. [41] ($\delta^{\mathrm{vp}} = 0.055$ for all studied energy points), and $\mathcal{L}_{\mathrm{int}}$ is the integrated luminosity at each energy point. The product of the D_s efficiency and branching fraction is $\epsilon_{D_s} = \epsilon\mathcal{B}(D_s^+ \to K^+K^-\pi^+)$ where ϵ is the detection efficiency and $\mathcal{B}(D_s^+ \to K^+K^-\pi^+)$ is the branching fraction for $D_s^+ \to K^+K^-\pi^+$ [36]. The calculation of the upper limits for Born cross sections at the 90% C.L. is performed analogously, replacing N_{fit} with $N_{\mathrm{U.L.}}$.

The measured Born cross sections of $e^+e^- \to D_s^+ D_{s1}(2460)^-$ and the corresponding upper limits at the 90% C.L. (with systematic uncertainties included) for the energy points with signal significances less than 3σ are summarized in Table I. The systematic uncertainties and the method to take them into account in the upper limits are discussed in Sec. VI. The Born cross sections with statistical error bars only are shown in Fig. 3, together with the fit result using the prediction of Ref. [10], i.e., $\sigma[e^+e^- \to D_s D_{s1}(2460)] \propto \sqrt{E_{\mathrm{c.m.}} - E_0}$. The fit gives $\chi^2/\mathrm{ndf} = 1.75$, where ndf is the number of degrees of freedom.

V. MEASUREMENT OF $e^+e^- \to D_s^{*+} D_{s1}(2460)^-$

In the events passing the selection criteria described in Sec. III, we search for $D_{s1}(2460)^-$ in the recoil mass of D_s^{*+}. To improve the mass resolution, mass-constrained fits to the nominal masses of D_s^+ and D_s^{*+} (2C) are applied. The χ^2_{2C} is required to be less than 10 to suppress background contributions. The recoil mass distributions of D_s^{*+} from data samples at $\sqrt{s} = 4.590$ GeV and 4.600 GeV are shown in Fig. 4. A clear $D_{s1}(2460)^-$ peak is observed at $\sqrt{s} = 4.600$ GeV, while there is no clear $D_{s1}(2460)^-$ signal at $\sqrt{s} = 4.590$ GeV. Detailed study of the generic MC samples indicates that there are no peaking background contributions in the $D_{s1}(2460)^-$ signal region [39]. The background events are from the processes with D^+D^{*-}, $D^0\bar{D}^{*0}$, $\pi^0 D^+ D^{*-}$, $\pi^- D^{*+}\bar{D}^0$, etc., in the final states.

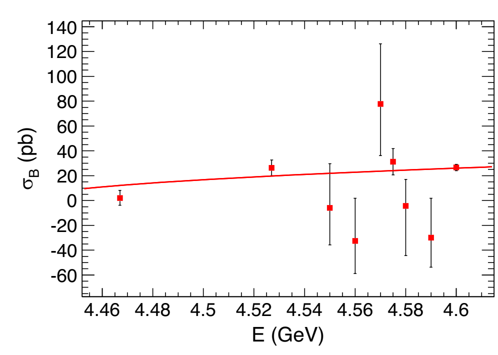

FIG. 3. The fit to the Born cross sections of $e^+e^- \to D_s^+ D_{s1}(2460)^-$ with $\sigma[e^+e^- \to D_s D_{s1}(2460)] \propto \sqrt{E_{\mathrm{c.m.}} - E_0}$. All error bars are statistical only.

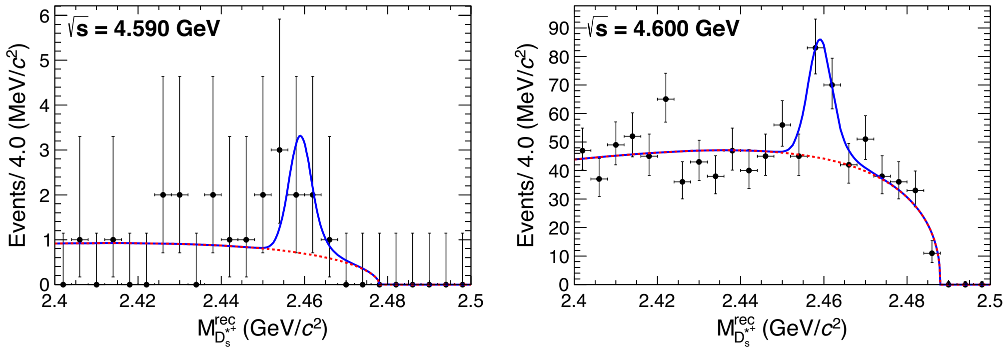

FIG. 4. The $M^{\rm rec}_{D_s^{*+}}$ distributions from data samples at $\sqrt{s} = 4.590$ GeV and 4.600 GeV, respectively; a clear $D_{s1}(2460)^-$ signal is seen at $\sqrt{s} = 4.600$ GeV. The dots with error bars are data, the solid line represents the best fit, and the dashed line represents the fitted background.

An unbinned maximum likelihood fit is performed to the $M^{\rm rec}_{D_s^{*+}}$ distribution in Fig. 4. The signal is described by a Crystal Ball function [42], the parameters of which are fixed to those obtained from the fit to the $M^{\rm rec}_{D_s^{*+}}$ distribution in the PHSP MC sample. The background is modeled with an ARGUS function [43]. The significances of the $D_{s1}(2460)^-$ signal at $\sqrt{s} = 4.590$ GeV and 4.600 GeV are 2.0σ and 5.9σ, respectively. The fit results together with the signal significances are summarized in Table I. The upper limit on the number of $D_{s1}(2460)^-$ signal events $N_{\rm U.L.}$ for $\sqrt{s} = 4.590$ GeV determined at the 90% C.L. is listed in Table I.

The Born cross section of $e^+e^- \to D_s^{*+}D_{s1}(2460)^-$ is calculated using the formula

$$\sigma_B(e^+e^- \to D_s^{*+}D_{s1}(2460)^-) = \frac{N_{\rm fit}}{\mathcal{L}_{\rm int}(1+\delta)(1+\delta^{\rm vp})\epsilon_{D_s^*}}. \tag{3}$$

Here, the parameters have the same meaning as in Eq. (2), except that $\epsilon_{D_s^*} = \epsilon^* \mathcal{B}(D_s^{*+} \to \gamma D_s^+)\mathcal{B}(D_s^+ \to K^+K^-\pi^+)$ where ϵ^* is the detection efficiency of the D_s^{*+} and $\mathcal{B}(D_s^{*+} \to \gamma D_s^+)$ is the branching fraction for $D_s^{*+} \to \gamma D_s^+$ [36].

The calculated Born cross sections of $e^+e^- \to D_s^{*+}D_{s1}(2460)^-$ at $\sqrt{s} = 4.590$ GeV and 4.600 GeV, and the upper limit at 90% C.L. (with systematic uncertainties included) for $\sqrt{s} = 4.590$ GeV are listed in Table I. The systematic uncertainties are discussed in Sec. VI.

VI. SYSTEMATIC UNCERTAINTIES

The systematic uncertainties on the measured cross sections of $e^+e^- \to D_s^+D_{s1}(2460)^-$ and $e^+e^- \to D_s^{*+}D_{s1}(2460)^-$ come from tracking and PID efficiencies, photon detection efficiency, and MC statistics. We also consider the uncertainties from ISR and vacuum polarization corrections, the luminosity measurement, branching fractions of intermediate states, the kinematic fit, MC generator, D_s^+ mass resolution, $M^{\rm rec}_{D_s^+}$ bin width, $D_{s1}(2460)^-$ mass, the background shape, and the fit range. These contributions to the systematic uncertainty are divided below into two categories: multiplicative systematic uncertainties and additive systematic uncertainties.

Multiplicative systematic uncertainties are analyzed as follows. The uncertainties of tracking and PID are determined to be 1.5%, 1.0%, and 1.0% for K^+, K^-, and π^+, respectively, using the control samples of $J/\psi \to p\bar{p}\pi^+\pi^-$ and $J/\psi \to K_S^0K^+\pi^-$, where the transverse momentum and angular region of the signal channels are taken into account. The uncertainty of the photon reconstruction efficiency is 1.0% per photon, which is derived from the study of $J/\psi \to \rho^0(\to \pi^+\pi^-)\pi^0(\to \gamma\gamma)$ [44]. The uncertainties due to MC statistics are determined to be at most 1.1% at each energy point. The shapes of the cross section of the processes $e^+e^- \to D_s^+D_{s1}(2460)^-$ and $e^+e^- \to D_s^{*+}D_{s1}(2460)^-$ affect the radiative correction factor and the detection efficiency. Due to the small number of data points with low statistics, a detailed determination of the energy dependence ("line shape"), which would allow for an iterative determination of radiative correction factors, is not possible. Therefore, we change the input line shapes to a simple polynomial form, and the differences in $\varepsilon(1+\delta)$ are taken as the systematic uncertainties. The uncertainty from the vacuum polarization factor is less than 0.1% [41], which is negligible compared to other sources of uncertainties. The integrated luminosities of the data samples are measured using large angle Bhabha scattering events with an uncertainty less than 1.0%. The uncertainties of $\mathcal{B}(D_s^+ \to K^+K^-\pi^+)$ and $\mathcal{B}(D_s^{*+} \to \gamma D_s^+)$ are 3.2% and 0.7%, respectively [36]. The uncertainty of the 2C kinematic fit is estimated using the control samples of $e^+e^- \to D_s^{*+}D_s^{*-}$ at $\sqrt{s} = 4.420$ GeV and 4.600 GeV. The difference in the data and MC efficiencies due to the addition of the 2C kinematic fit requirement is 1.7%, which is taken as the systematic uncertainty. Signal MC samples are generated with a PHSP model. We also generate signal MC samples with a polar angle distribution of $1+\cos^2\theta$ or

TABLE II. Summary of systematic uncertainties of the Born cross sections of $e^+e^- \to D_s^+ D_{s1}(2460)^-$ and $e^+e^- \to D_s^{*+} D_{s1}(2460)^-$ for those energy points with statistical significances larger than 3σ.

Sources	$e^+e^- \to D_s^+ D_{s1}(2460)^-$			$e^+e^- \to D_s^{*+} D_{s1}(2460)^-$
$\sqrt{s}$ (GeV)	4.527	4.575	4.600	4.600
Tracking, PID and photon	3.5%	3.5%	3.5%	3.7%
MC statistics	0.5%	0.5%	0.5%	1.0%
ISR correction	4.6%	8.2%	5.5%	0.1%
Luminosity	0.7%	0.7%	0.7%	0.7%
Branching fraction	3.2%	3.2%	3.2%	3.3%
Kinematic fit	⋯	⋯	⋯	1.7%
MC generator	1.3%	1.3%	1.3%	1.7%
D_s^+ mass resolution	1.3%	4.4%	1.5%	⋯
$M^{\rm rec}_{D_s^+}$ bin width	6.1%	13.6%	1.5%	⋯
$D_{s1}(2460)^-$ mass	0.9%	11.8%	2.6%	⋯
Background shape	2.9%	5.5%	4.1%	1.7%
Fit range	2.5%	5.6%	1.1%	5.9%
Total	10.1%	22.3%	9.2%	8.3%

$1-\cos^2\theta$ for the D_s^+/D_s^{*+} meson. The maximum differences in detection efficiencies are 1.3% and 1.7% for the reconstructed D_s^+ and D_s^{*+} candidates.

Additive systematic uncertainties due to the fit are analyzed as follows. The uncertainty due to the D_s^+ mass resolution is estimated by varying this mass resolution by $\pm 1\sigma$ when fitting the $K^+K^-\pi^+$ invariant mass distributions in $M^{\rm rec}_{D_s^+}$ bins. The differences in the fitted $D_{s1}(2460)^-$ signal yields are taken as the systematic uncertainties. The uncertainties due to the $M^{\rm rec}_{D_s^+}$ bin width are studied by varying the $M^{\rm rec}_{D_s^+}$ bin width from 4.0 MeV$/c^2$ to 5.0 MeV$/c^2$. The differences in the fitted $D_{s1}(2460)^-$ signal yields are taken as the systematic uncertainties. The uncertainties due to the $D_{s1}(2460)^-$ mass are obtained by varying the $D_{s1}(2460)^-$ mass by $\pm 1\sigma$, i.e., 0.6 MeV$/c^2$ [36], in the fit of the $M^{\rm rec}_{D_s^+}$ distribution. The difference in the fitted $D_{s1}(2460)^-$ signal yields is taken as the systematic uncertainty. In the analysis of $e^+e^- \to D_s^+ D_{s1}(2460)^-$, the uncertainties attributed to the background shape are estimated by using different background shapes: (1) a first-order polynomial is used as the background shape (for $\sqrt{s} = 4.527$ GeV and 4.600 GeV data samples, a third-order polynomial is used as the background shape); (2) a second-order polynomial and the normalized contribution from $e^+e^- \to D_s^{*+} D_s^{*-}$ are used as the total background shape. In the analysis of $e^+e^- \to D_s^{*+} D_{s1}(2460)^-$, the uncertainties due to the background shape are estimated by using a parametrized polynomial $f(M) = (M - M_a)^c (M_b - M)^d$ instead of an ARGUS function [43], where M_a and M_b are the lower and upper thresholds of the D_s^{*+} recoil mass distribution. The maximum differences in the fitted $D_{s1}(2460)^-$ signal yields are considered as the systematic uncertainties. In the analysis of $e^+e^- \to D_s^+ D_{s1}(2460)^-$, the uncertainties due to the fit range are obtained by varying the fit range by 10 MeV on the left or right side. In the analysis of $e^+e^- \to D_s^{*+} D_{s1}(2460)^-$, the uncertainties due to the fit range are determined by varying the fit

TABLE III. Summary of multiplicative systematic uncertainties of the Born cross sections of $e^+e^- \to D_s^+ D_{s1}(2460)^-$ and $e^+e^- \to D_s^{*+} D_{s1}(2460)^-$ for those energy points with statistical significances less than 3σ.

Sources	$e^+e^- \to D_s^+ D_{s1}(2460)^-$						$e^+e^- \to D_s^{*+} D_{s1}(2460)^-$
$\sqrt{s}$ (GeV)	4.467	4.550	4.560	4.570	4.580	4.590	4.590
Tracking, PID and photon	3.5%	3.5%	3.5%	3.5%	3.5%	3.5%	3.7%
MC statistics	0.5%	0.5%	0.5%	0.5%	0.5%	0.5%	1.1%
ISR correction	13.1%	7.6%	8.1%	2.8%	7.6%	7.0%	1.6%
Luminosity	0.7%	0.8%	0.8%	0.8%	0.7%	0.7%	0.7%
Branching fraction	3.2%	3.2%	3.2%	3.2%	3.2%	3.2%	3.3%
Kinematic fit	⋯	⋯	⋯	⋯	⋯	⋯	1.7%
MC generator	1.3%	1.3%	1.3%	1.3%	1.3%	1.3%	1.7%
Total	14.0%	9.1%	9.5%	5.7%	9.1%	8.6%	5.7%

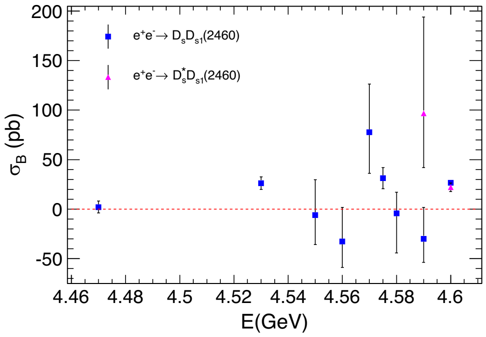

FIG. 5. The comparison of the Born cross sections of $e^+e^- \to D_s^+ D_{s1}(2460)^-$ (squares with error bars) and $e^+e^- \to D_s^{*+} D_{s1}(2460)^-$ (triangles with error bars), where the error bars are statistical only.

range from $[2.40, 2.49]$ GeV$/c^2$ to $[2.30, 2.49]$ GeV$/c^2$. The differences in the fitted $D_{s1}(2460)^-$ signal yields are taken as the systematic uncertainties.

For those energy points with a statistical significance larger than 3σ, the central values of the cross section with statistical and systematic uncertainties are reported, and all of the systematic uncertainties are summarized in Table II. For the other energy points with $D_{s1}(2460)^-$ signal significance less than 3σ, the upper limits on the cross section at the 90% C.L. are reported and the systematic uncertainties are taken into account in two steps. First, when we study the additive systematic uncertainties described above, we take the most conservative upper limit at the 90% C.L. on the number of $D_{s1}(2460)^-$ signal yields. Then, to take into account the multiplicative systematic uncertainty, the likelihood with the most conservative upper limit is convolved with a Gaussian function, with a width equal to the corresponding total multiplicative systematic uncertainty. All of the multiplicative systematic uncertainties for the energy points with $D_{s1}(2460)^-$ signal significance less than 3σ are summarized in Table III. Assuming that all the sources are independent, the total systematic uncertainty is obtained by adding them in quadrature. The final results of the Born cross section with systematic uncertainties considered are listed in Table I. The comparison of the Born cross sections of $e^+e^- \to D_s^+ D_{s1}(2460)^-$ and $e^+e^- \to D_s^{*+} D_{s1}(2460)^-$ is shown in Fig. 5 with statistical error bars only.

VII. SUMMARY

In summary, we observe $D_{s1}(2460)^-$ signals with statistical significances larger than 3σ in the processes $e^+e^- \to D_s^+ D_{s1}(2460)^-$ $(e^+e^- \to D_s^{*+} D_{s1}(2460)^-)$ at c.m. energies of 4.527 GeV, 4.575 GeV, and 4.600 GeV (4.600 GeV). The Born cross sections, $\sigma_B[e^+e^- \to D_s^+ D_{s1}(2460)^-]$ and $\sigma_B[e^+e^- \to D_s^{*+} D_{s1}(2460)^-]$, have been measured for the first time and displayed in Fig. 5. The prediction on the energy dependence of the Born cross section given in Ref. [10], i.e., $\sigma[e^+e^- \to D_s D_{s1}(2460)] \propto \sqrt{E_{\mathrm{c.m.}} - E_0}$, is confronted with the result of our measurement in Fig. 3. Within the statistical uncertainty of the measurement, the theoretical prediction can describe the data.

ACKNOWLEDGMENTS

The BESIII collaboration thanks the staff of BEPCII and the IHEP computing center for their strong support. This work is supported in part by National Key Basic Research Program of China under Contract No. 2015CB856700; National Natural Science Foundation of China (NSFC) under Contracts No. 11625523, No. 11635010, No. 11735014, No. 11822506, No. 11835012, No. 11935015, No. 11935016, No. 11935018, No. 11961141012; the Chinese Academy of Sciences (CAS) Large-Scale Scientific Facility Program; Joint Large-Scale Scientific Facility Funds of the NSFC and CAS under Contracts No. U1732263, No. U1832207; CAS Key Research Program of Frontier Sciences under Contracts No. QYZDJ-SSW-SLH003, No. QYZDJ-SSW-SLH040; 100 Talents Program of CAS; INPAC and Shanghai Key Laboratory for Particle Physics and Cosmology; ERC under Contract No. 758462; German Research Foundation DFG under Contracts Nos. Collaborative Research Center CRC 1044, FOR 2359; Istituto Nazionale di Fisica Nucleare, Italy; Ministry of Development of Turkey under Contract No. DPT2006K-120470; National Science and Technology fund; STFC (United Kingdom); The Knut and Alice Wallenberg Foundation (Sweden) under Contract No. 2016.0157; The Royal Society, UK under Contracts No. DH140054, No. DH160214; The Swedish Research Council; U.S. Department of Energy under Contracts No. DE-FG02-05ER41374, No. DE-SC-0012069.

[1] D. Besson *et al.* (CLEO Collaboration), Phys. Rev. D **68**, 032002 (2003).
[2] P. Krokovny *et al.* (Belle Collaboration), Phys. Rev. Lett. **91**, 262002 (2003).
[3] B. Aubert *et al.* (*BABAR* Collaboration), Phys. Rev. D **69**, 031101 (2004).
[4] S. Godfrey and N. Isgur, Phys. Rev. D **32**, 189 (1985).

[5] J. Zeng, J. W. Van Orden, and W. Roberts, Phys. Rev. D **52**, 5229 (1995).
[6] A. Faessler, T. Gutsche, V. E. Lyubovitskij, and Y.-L. Ma, Phys. Rev. D **76**, 114008 (2007).
[7] M. Cleven, H. W. Grießhammer, F.-K. Guo, C. Hanhart, and U.-G. Meißner, Eur. Phys. J. A **50**, 149 (2014).
[8] C. J. Xiao, D. Y. Chen, and Y. L. Ma, Phys. Rev. D **93**, 094011 (2016).
[9] P. G. Ortega, J. Segovia, D. R. Entem, and F. Fernández, Eur. Phys. J. Web Conf. **130**, 02009 (2016).
[10] M. B. Voloshin, Phys. Lett. B **783**, 175 (2018).
[11] B. Aubert *et al.* (*BABAR* Collaboration), Phys. Rev. Lett. **95**, 142001 (2005).
[12] T. E. Coan *et al.* (CLEO Collaboration), Phys. Rev. Lett. **96**, 162003 (2006).
[13] C. Z. Yuan *et al.* (Belle Collaboration), Phys. Rev. Lett. **99**, 182004 (2007).
[14] B. Aubert *et al.* (*BABAR* Collaboration), Phys. Rev. Lett. **98**, 212001 (2007).
[15] X. L. Wang *et al.* (Belle Collaboration), Phys. Rev. Lett. **99**, 142002 (2007).
[16] G. Pakhlova *et al.* (Belle Collaboration), Phys. Rev. D **83**, 011101 (2011).
[17] P. del Amo Sanchez *et al.* (*BABAR* Collaboration), Phys. Rev. D **82**, 052004 (2010).
[18] D. Cronin-Hennessy *et al.* (CLEO Collaboration), Phys. Rev. D **80**, 072001 (2009).
[19] M. Ablikim *et al.* (BESIII Collaboration), Chin. Phys. C **43**, 031001 (2019).
[20] S. Jia *et al.* (Belle Collaboration), Phys. Rev. D **100**, 111103 (R) (2019).
[21] S. Jia *et al.* (Belle Collaboration), Phys. Rev. D **101**, 091101 (R) (2020).
[22] M. Ablikim *et al.* (BESIII Collaboration), Nucl. Instrum. Methods Phys. Res., Sect. A **614**, 345 (2010).
[23] J. Z. Bai *et al.* (BES Collaboration), Nucl. Instrum. Methods Phys. Res., Sect. A **344**, 319 (1994).
[24] M. Ablikim *et al.* (BESIII Collaboration), Chin. Phys. C **40**, 063001 (2016).
[25] M. Ablikim *et al.* (BESIII Collaboration), Chin. Phys. C **39**, 093001 (2015).
[26] M. Ablikim *et al.* (BESIII Collaboration), Chin. Phys. C **41**, 063001 (2017).
[27] S. Agostinelli *et al.* (GEANT4 Collaboration), Nucl. Instrum. Methods Phys. Res., Sect. A **506**, 250 (2003).
[28] Z. Y. Deng *et al.*, Chin. Phys. C **30**, 371 (2006), http://cpc.ihep.ac.cn/en/article/id/283d17c0-e8fa-4ad7-bfe3-92095466def1.
[29] S. Jadach, B. F. L. Ward, and Z. Was, Comput. Phys. Commun. **130**, 260 (2000).
[30] R. G. Ping, Chin. Phys. C **38**, 083001 (2014).
[31] S. Jadach, B. F. L. Ward, and Z. Was, Phys. Rev. D **63**, 113009 (2001).
[32] R. G. Ping, Chin. Phys. C **32**, 599 (2008).
[33] D. J. Lange, Nucl. Instrum. Methods Phys. Res., Sect. A **462**, 152 (2001).
[34] P. Golonka and Z. Was, Eur. Phys. J. C **45**, 97 (2006).
[35] R. E. Mitchell *et al.* (CLEO Collaboration), Phys. Rev. D **79**, 072008 (2009).
[36] M. Tanabashi *et al.* (Particle Data Group), Phys. Rev. D **98**, 030001 (2018).
[37] L. C. Chen, G. S. Huang, X. R. Qi, D. H. Zhang, and Y. S. Zhu, Phys. Rev. D **62**, 034003 (2000).
[38] T. Sjöstrand, S. Ask, J. R. Christiansen, R. Corke, N. Desai, P. Ilten, S. Mrenna, S. Prestel, C. O. Rasmussen, and P. Z. Skands, Comput. Phys. Commun. **191**, 159 (2015).
[39] X. Y. Zhou, S. X. Du, G. Li, and C. P. Shen, arXiv:2001.04016.
[40] E. A. Kuraev and V. S. Fadin, Yad. Fiz. **41**, 733 (1985).
[41] F. Jegerlehner, Nuovo Cimento Soc. Ital. Fis. **34C**, 31 (2011).
[42] T. Skwarnicki, Ph.D. thesis, Institute for Nuclear Physics, 1986; DESY Internal Report No. DESY F31-86-02, 1986.
[43] H. Albrecht *et al.* (ARGUS Collaboration), Phys. Lett. B **340**, 217 (1994).
[44] M. Ablikim *et al.* (BESIII Collaboration), Phys. Rev. D **81**, 052005 (2010).